Numerical Study on the Effect of Natural Gas on Aircraft Turbofan Engine Propulsion

Tarek M. Belal[1,*] and El Sayed M. Marzouk[2]

[1]*Department of Mechanical Engineer, Pharos University, Alexandria, Egypt*

[2]*Department of Mechanical Engineering, Umm Al-Qura University, Makka, KSA*

Abstract: The world has been concerned and worried about the depletion of the liquid oil fuel, besides new environmental rules are to be followed to reduce pollution hazards and global warming. The utilization of natural gas (as a near term fuel) and hydrogen (as long-term fuel) are receiving great attention, because they have less pollution effects. Since the aviation has a great deal in environmental pollution effects due to the cruise flight in the upper troposphere (supersonic aircraft) or in the lower stratosphere (subsonic aircraft) where most of the ozone concentrate, which helps in protecting the earth form ultra violet radiation. Therefore, the use of alternate fuel has a great attention in aviation. In the present study, the thrust specific fuel consumption and specific thrust for the aircraft during aircraft flight profile are predicted, when using aviation fuel and natural gas. The P&W JT9D –7R-turbofan jet engine is taken as a base line engine propelling the Boeing 747-200 aircraft as a base line aircraft with four engine nacelles mounted on wings. The model engine fuel-air cycle representation is carried out for design point calculations based on sea level static conditions and variable specific heats along engine components. The predicted engine performance results compared very well with the reported values by the manufacture. Predictions carried out using aviation fuel and natural gas show an increase in the specific thrust by 3% and decrease in the thrust specific fuel consumption by 14% and fuel to air ratio by 11%, when using natural gas.

Keywords: Aviation, boeing, combustion ,dimensionless analysis , fuel, natural gas, P&W JT9D-R, performance ,specific fuel consumptions, specific heat, specific thrust, T-S chart, turbofan.

1. INTRODUCTION

Air transportation plays a substantial role in world economic activity, and society relies heavily on the benefits associated with aviation. The commercial sector of the industry is highly competitive, consisting in 1994 of about 15,000 aircraft operating over routes of approximately 15 million-km in total length and serving nearly 10,000 airports. In 1994, more than 1.25 billion passengers used the world's airlines for business and vacation travel, and well in excess of a third of the value of the world's manufactured exports were transported by air [1]. Aircraft perturb the atmosphere by changing background levels of trace gases and particles and by forming condensation trails (contrails). Aircraft emissions include greenhouse gases such as CO_2 and H_2O that trap terrestrial radiation and chemically active gases that alter natural greenhouse gases, such as O_3 and CH_4. Particles may directly interact with the Earth's radiation balance or influence the formation and radiative properties of clouds. There is a range of options to reduce the impact of aviation emissions, including changes in aircraft and engine technology, fuel, operational practices, and regulatory and economic measures. In the present study, the fuel option will be the main concern. Jet aircraft require fuel with a high energy density, especially for long-haul flights. Other fuel options, such as natural gas may be viable in the short term, but would require new aircraft fuel system designs and new infrastructures for supply. The option of changing the fuel is coincidence with the danger of fuel oil high prices and depletion by 2050 [2]. Fundamental flame holding and combustion tests using simple V-gutters for the flame holders were investigated in order to obtain basic design data of a natural gas fueled ram combustor. The results indicate that high combustion efficiency is attainable, when controlling the concentration of methane air mixture flowed into a flame holder even at a low equivalence ratio [3]. Experiments were conducted investigating the influence of modifications in combustion chambers of gas turbine engines on completeness of combustion and the emission of toxic gases. The characteristics of the toxic exhaust gases of the NK-12CT turbofan engine with two types of fuel sprayers were determined for the case of methane combustion. It is shown that replacing fluidic-gas sprayers with centrifugal sprayers reduces the emission of nitrogen oxides by 40-50% [4]. A method is proposed for estimating the energy efficiency of the combustion chambers of gas turbine engines operating on natural gas. Varying the air velocity at the inlet can optimize the combustion process. It is calculated that optimum inlet air velocity of 95-100 m/s, is practically equal to the velocity adopted in the case of kerosene fuel [5]. The annular combustion chamber of a NK-8 turbofan engine was

*Address correspondence to this author at the Department of Mechanical Engineer, Pharos University, Alexandria, Egypt; Tel: +201225707351; Fax: +2035827131; E-mail: tarek.belal@pua.edu.eg

E-ISSN: 2409-9848/14

studied during combustion of natural gas. It showed good combustion performance even at high air inlet velocity (120-130 m/s) [6]. The use of natural gas as an alternative fuel for aviation gas turbine engines can significantly reduce the amount of cancerogenic compounds released into the atmosphere. At all operating regimes, the relative amount of the released benz pyrene, one of the strongest and most stable cancerogens, contained in the exhaust gases, is a factor of 3-4 lower than in the case of kerosene-burning engines [7]. Several flight tests had been done on different aircraft configuration supplied with natural gas fuel, to achieve the aircraft and engine design and off design conditions of aviation fuel. The US bomber B-57D was the first cryogenic fuel used aircraft in 1956, designed to fueled with liquid hydrogen [8]. The Tu-155 powered by one engine fueled by liquid hydrogen, kerosene and liquid natural gas has performed actual flight tests in 1990, and has shown the real possibility of cryogenic evaluation creation [9]. Thomas, C.E. introduced the aircraft A310 airbus, which is the next century European aircraft uses liquid hydrogen, kerosene and liquid natural gas as near term fuel [10].

2. MATHEMATICAL MODEL

In actual engine cycle, the working fluid is air being compressed and then changes into combustion gases. The specific heats of the constituent of the working fluid changes with temperature. The products of combustion may be subjected to certain dissociation at high temperature. If the actual physical properties of the gases before and after combustion are taken into account, a reasonably close value of actual pressures, temperatures exiting within engine can be estimated. The analysis based on these actual properties of the working fluid is the fuel-air cycle analysis, which takes into account the following:

- Actual, which affects the complete combustion of air and fuel at high temperature above composition of the gases through the engine's different component.
- Variation of specific heats and specific heat ratio variation with temperature.
- The effect of dissociation nearly 1700 K, which leads to presence of CO, H_2, at equilibrium conditions.
- Variation in the number of molecules upon combustion.
- Subsequent to combustion, which is assumed to take, place instantaneously upon fuel introduction in the combustion chamber. The charge is assumed to be always in chemical equilibrium.
- The processes in different engine components are assumed to be adiabatic.

The thermodynamics equations of state for perfect gas are:

$$\mathbf{P=\rho RT} \quad (1)$$

$$\mathbf{u=}\mathit{f}\mathbf{(T)} \quad (2)$$

$$h = \mathit{f}\,(T). \quad (3)$$

For a hydrocarbon fuel, the chemical composition is $\mathbf{C_a\ H_b}$, and then the combustion equation becomes:

$$C_a H_b + n_{O2}\lambda\,(O_2+3.7619N_2) \rightarrow n_{CO2}\,CO_2 + n_{H2O}\,H_2O + n_{O2}\,(\lambda -1)\,O_2 + n_{N2}\,\lambda\,N_2 \quad (4)$$

$$C_{12}H_{23} + 17.75(O_2 + 3.7619N_2) \rightarrow 12\,CO_2 + 11.5\,H_2O + 66.7737N_2 \quad (5)$$

$$CH_4 + 2(O_2 + 3.7619N_2) \rightarrow CO_2+2H_2O+7.5238N_2 \quad (6)$$

Temperature-entropy chart consists of energy lines and group of constant pressure specific entropy lines and others constant volume specific entropy lines. The main assumptions used when plotting the T-S chart are given together with the method of construction of the energy lines and entropy lines at constant pressure or constant volume.

- No dissociation occurs during combustion, as excess air factor is high while maximum cycle temperature is less than 1700K.
- All the mixture reactants and products of combustion behave as perfect gases.
- Variation of specific heat with pressure is neglected and gases are thermally perfect gases.
- The specific heats at constant pressure are available in thermodynamic data Tables, published by the national bureau of standard called "JANAF" Tables (1971) [14].
- For computer calculation it is awkward to deal with tabular data, for this reason, specific heats at constant pressure are curve fitted by help of a software package called Matlab. The data are divided into two groups, from 0 to 1000K, and from 1000 to 2000K. The results of the fitted curves are tested to be almost identical to the related "JANAF" Tables [14].

Table 1: Applied from 0K to 1000K

Constant	H_2O	O_2	N_2	CO_2
A_0	1.0876E-08	1.4744E-08	1.4909E-08	-3.3382E-08
A_1	2.3184E-01	2.0230E-01	2.0400E-01	2.1484E-01
A_2	-2.7660E-03	-2.4079E-03	-2.4523E-03	-2.7815E-03
A_3	1.8152E-05	1.5759E-05	1.6205E-05	1.9832E-05
A_4	-7.3546E-08	-6.3708E-08	-6.5988E-08	-8.4534E-08
A_5	1.9409E-10	1.6791E-10	1.7452E-10	2.2995E-10
A_6	-3.3984E-13	-2.9386E-13	-3.0557E-13	-4.1024E-13
A_7	3.9163E-16	3.3861E-16	3.5166E-16	4.7852E-16
A_8	-2.8538E-19	-2.4676E-19	-2.5573E-19	-3.5157E-19
A_9	1.1913E-22	1.0303E-22	1.0651E-22	1.4763E-22
A_{10}	-2.1697E-26	-1.8770E-26	-1.9355E-26	-2.7008E-26

Table 2: Applied from 1000K to 2000K

Constant	H_2O	O_2	N_2	CO_2
A_0	7.2616E+04	8.8555E+03	-6.6143E+05	7.2962E+03
A_1	-5.2441E+02	-6.1575E+01	4.6720E+03	-5.5026E+01
A_2	1.6965E+00	1.9168E-01	-1.4764E+01	1.8504E-01
A_3	-3.2375E-03	-3.5152E-04	2.7488E-02	-3.6498E-04
A_4	4.0361E-06	4.2060E-07	-3.3392E-05	4.6778E-07
A_5	-3.4347E-09	-3.4312E-10	2.7657E-08	-4.0720E-10
A_6	2.0207E-12	1.9329E-13	-1.5817E-11	2.4388E-13
A_7	-8.1158E-16	-7.4247E-17	6.1681E-15	-9.9256E-17
A_8	2.1297E-19	1.8614E-20	-1.5697E-18	2.6279E-20
A_9	-3.2972E-23	-2.7502E-24	2.3542E-22	-4.0881E-24
A_{10}	2.2873E-27	1.8188E-28	-1.5801E-26	2.8384E-28

The function that apply for any given species in the polynomial form is:

$$Cp(T) = A_o + A_1T + A_2T^2 + A_3T^3 + A_4T^4 + A_5T^5 + A_6T^6 + A_7T^7 + A_8T^8 + A_9T^9 + A_{10}T^{10} \quad (7)$$

The constants of the important species are given in Table (**1** and **2**). Below are the thermodynamics models for the specific heat, molecular weight, internal energy, flow work and enthalpy per mole combustion gases.

$$Cp_{cg}(T) = \sum_{i=1}^{j} \chi_i Cp_i(\mathrm{T}) \quad (8)$$

$$M_{cg}(f) = \sum_{i=1}^{j} \chi_i M_i \quad (9)$$

$$u_{cg}(T) = \sum_{i=1}^{j} \chi_i \int_{T_o}^{T} \left(Cp_i(T) - R\right) dT \quad (10)$$

$$RT(T) = \sum_{i=1}^{j} \chi_i \int_{T_o}^{T} R \, \mathrm{dT} \quad (11)$$

$$h_{cg}(T) = \sum_{i=1}^{j} \chi_i \int_{T_o}^{T} Cp_i(\mathrm{T}) \, dT \quad (12)$$

In addition, the line of entropy per mole combustion gases are calculated as follow:

$$s_{p_{cg}}(T,p) = \sum_{i=1}^{j} \chi_i \left(\int_{T_o}^{T} \left(\frac{Cp_i(T)}{T} \right) \mathrm{dT} - \mathrm{R} \int_{p_o}^{p} \frac{dp}{p} \right) \quad (13)$$

$$s_{v_{cg}}(T,v) = \sum_{i=1}^{j} \chi_i \left(\int_{T_o}^{T} \left(\frac{Cp_i(T) - R}{T} \right) \mathrm{dT} + \mathrm{R} \int_{v_o}^{v} \frac{dv}{v} \right) \quad (14)$$

Figure (**2, 4, 3**) and (**5**) show demonstration of the computer program run calculating the T-S chart for air and combustion gases using conventional aviation fuel

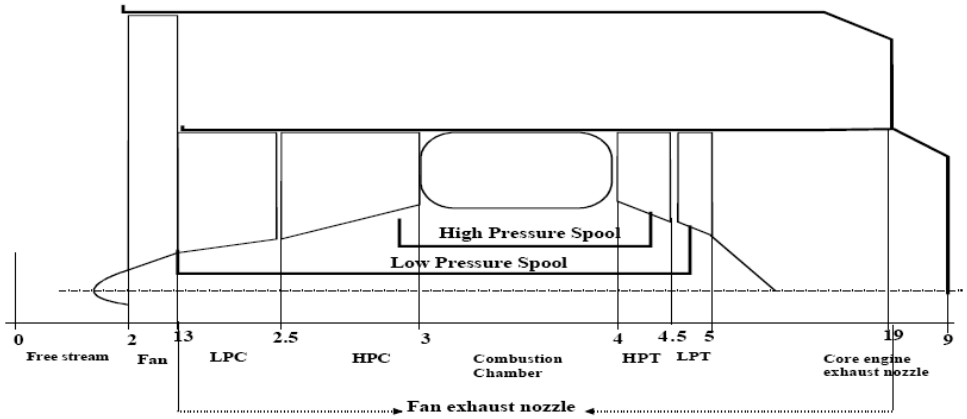

Figure 1: JT9D-7R turbofan engine schematic diagram.

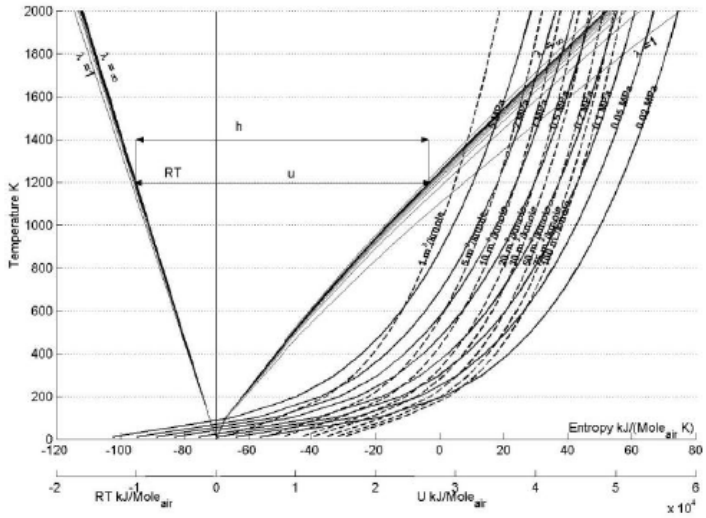

Figure 2: T-S chart of aviation fuel per mole air.

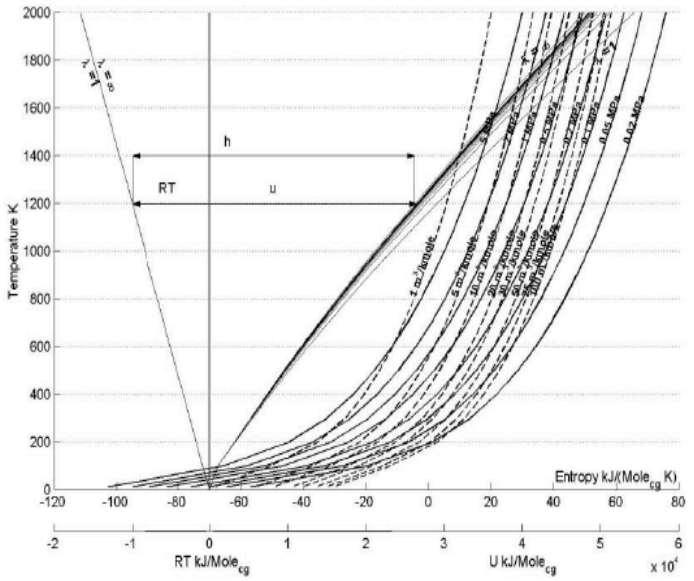

Figure 3: T-S chart of aviation fuel per mole combustion gases.

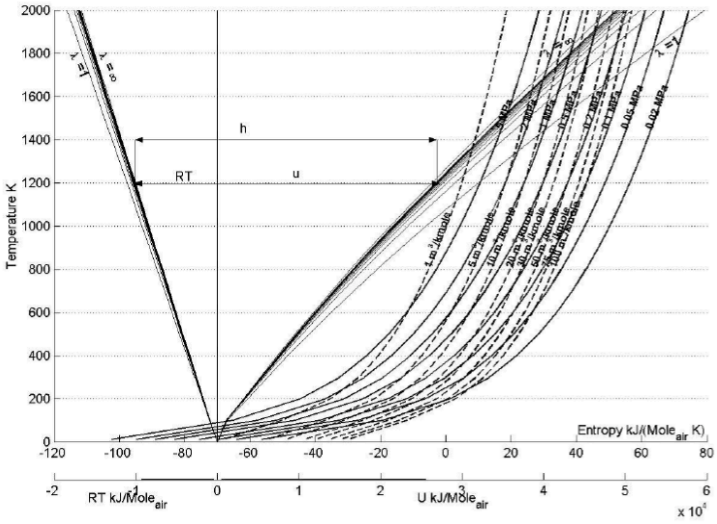

Figure 4: T-S chart of natural gas fuel per mole air.

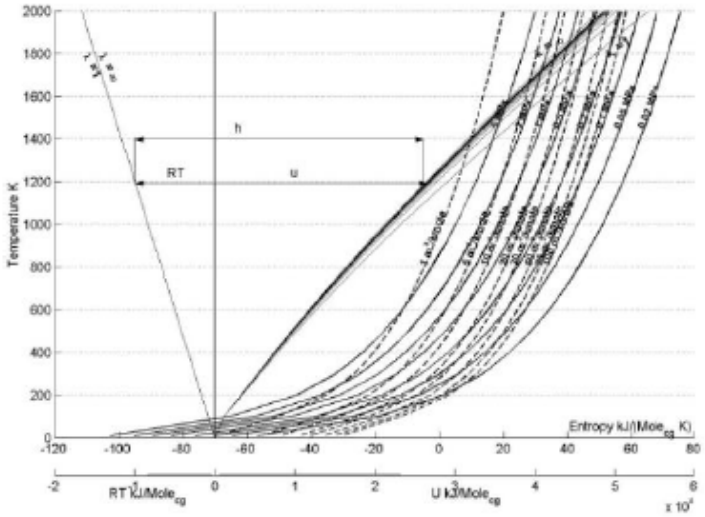

Figure 5: T-S chart of natural gas fuel per mole combustion gases.

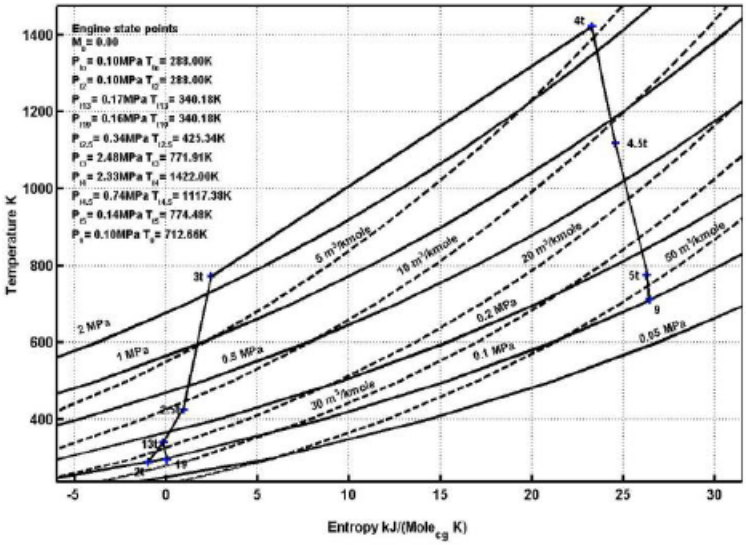

Figure 6: JT9D-7R turbofan engine cycle using aviation fuel.

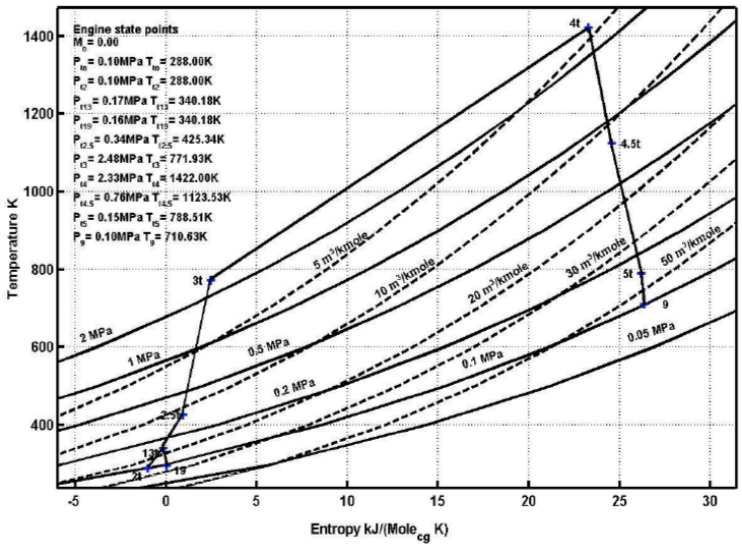

Figure 7: JT9D-7R turbofan engine cycle using natural gas fuel.

and natural gas fuel respectively. Figures (**6**) and (**7**) show the turbofan engine cycle on T-S chart (using aviation fuel and natural gas respectively) of the core engine and the fan bypass. The engine section's number referenced in Figure (**1**) .The assumptions for the analysis of the turbofan cycle with losses are as follows:

- Perfect gas upstream of main burner.
- Perfect gas downstream of main burner.
- The specific heats through all engine components are variable with temperature.
- All components are adiabatic.
- The efficiency of the fan, compressor and turbine are described through

$$\tau_f = \frac{h_{t_{13}}}{h_{t_2}} \tag{15}$$

$$\pi_f = \frac{P_{t_{13}}}{P_{t_2}} w \tag{16}$$

From the definition of the polytropic efficiency

$$e_f = R\frac{dP_t/P_t}{dh_t/T_t} \tag{17}$$

$$\pi_f = \frac{P_{t_{13}}}{P_{t_2}} = \exp\left(e_f \frac{\phi_{t_{13}} - \phi_{t_2}}{R}\right) \tag{18}$$

Where $\phi = \int_{T_{ref}}^{T} \frac{C_p(T)dT}{T}$,

$$\eta_f = \frac{h_{t_{13i}} - h_{t_2}}{h_{t_{13}} - h_{t_2}} \tag{19}$$

For the low-pressure compressor variables τ_{cL} and π_{cL} will be predicted as for fan stream variables.

$$\tau_{c_L} = \frac{h_{t_{2.5}}}{h_{t_2}} \tag{20}$$

$$\pi_{c_L} = \frac{P_{t_{2.5}}}{P_{t_2}} = \exp\left(e_{c_L} \frac{\phi_{t_{2.5}} - \phi_{t_2}}{R}\right) \tag{21}$$

Where components polytropic efficiencies are selected from Figure of merits based on level of technology [13], and the low-pressure compressor isentropic efficiency can be expressed as follows:

$$\eta_{c_L} = \frac{h_{t_{2.5i}} - h_{t_2}}{h_{t_{2.5}} - h_{t_2}} \tag{22}$$

For the high-pressure compressor

$$\tau_{c_H} = \frac{h_{t_3}}{h_{t_{2.5}}} \tag{23}$$

$$\pi_{c_H} = \frac{P_{t_3}}{P_{t_{2.5}}} = \exp\left(e_{c_H} \frac{\phi_{t_3} - \phi_{t_{2.5}}}{R}\right) \tag{24}$$

The high-pressure compressor isentropic efficiency can be expressed as follows:

$$\eta_{c_H} = \frac{h_{t_{3i}} - h_{t_{2.5}}}{h_{t_3} - h_{t_{2.5}}} \tag{25}$$

For the main burner

$$\tau_b = \frac{h_{t_4}}{h_{t_3}} \tag{26}$$

$$\pi_b = \frac{P_{t_4}}{P_{t_3}} \tag{27}$$

From the definition of the main burner efficiency, we can define the fuel to air ratio as:

$$f = \frac{h_{t_4} - h_{t_3}}{\eta_b h_{PR} - h_{t_4}} \tag{28}$$

The application of the first law of the thermodynamics to the high-pressure compressor and high-pressure turbine (high-pressure spool) gives the required turbine exit enthalpy. Equating the required compressor power to the net output power from the turbine, and rewriting in terms of mass flow rates and total enthalpies gives:

$$\begin{aligned} &\overset{\circ}{m}_C\left(h_{t_3} - h_{t_{2.5}}\right) = \eta_{m_H}\left(\overset{\circ}{m}_C + \overset{\circ}{m}f\right)\left(h_{t_4} - h_{t_{4.5}}\right) \\ &= \eta_{m_H}(1+f)\left(h_{t_4} - h_{t_{4.5}}\right) \end{aligned} \tag{29}$$

$$h_{t_{4.5}} = h_{t_4} - \frac{h_{t_3} - h_{t_{2.5}}}{(1+f)\eta_{m_H}} \tag{30}$$

Then

$$\tau_{t_H} = \frac{h_{t_{4.5}}}{h_{t_4}} \tag{31}$$

$$\pi_{t_H} = \frac{P_{t_{4.5}}}{P_{t_4}} = \exp\left(\frac{\phi_{t_{4.5}} - \phi_{t_4}}{Re_{t_H}}\right) \tag{32}$$

The high-pressure turbine isentropic efficiency can predict from

$$\eta_{t_H} = \frac{h_{t_4} - h_{t_{4.5}}}{h_{t_4} - h_{t_{4.5i}}} \tag{33}$$

The application of the first law of the thermodynamics to the fan, low-pressure compressor and low-pressure turbine (low-pressure spool) gives the required turbine exit enthalpy. Equating the required fan and low-pressure compressor power to the net output power from the low-pressure turbine, and rewriting in terms of mass flow rates and total enthalpies gives:

$$\begin{aligned} &\overset{\circ}{m}_C\left(h_{t_{2.5}} - h_{t_2}\right) + \overset{\circ}{m}_F\left(h_{t_{13}} - h_{t_2}\right) = \eta_{m_L}\left(\overset{\circ}{m}_C + \overset{\circ}{m}f\right)\left(h_{t_{4.5}} - h_{t_5}\right) \\ &\left(h_{t_{2.5}} - h_{t_2}\right) + \alpha\left(h_{t_{13}} - h_{t_2}\right) = \eta_{m_H}(1+f)\left(h_{t_{4.5}} - h_{t_5}\right) \end{aligned} \tag{34}$$

$$h_{t_5} = h_{t_{4.5}} - \frac{\left(h_{t_{2.5}} - h_{t_2}\right) + \alpha\left(h_{t_{13}} - h_{t_2}\right)}{(1+f)\eta_{m_H}} \tag{35}$$

Then

$$\tau_{t_L} = \frac{h_{t_5}}{h_{t_{4.5}}} \tag{36}$$

and from polytropic efficiency definition we have:

$$\pi_{t_L} = \frac{P_{t_5}}{P_{t_{4.5}}} = \exp\left(\frac{\phi_{t_5} - \phi_{t_{4.5}}}{Re_{t_L}}\right) \tag{37}$$

The low-pressure turbine isentropic efficiency can predict from

$$\eta_{t_L} = \frac{h_{t_{4.5}} - h_{t_5}}{h_{t_{4.5}} - h_{t_{5i}}} \tag{38}$$

The nozzles is assumed to be adiabatic, then for the core engine exhaust nozzle we have

$$\tau_n = \frac{h_{t_9}}{h_{t_5}} = 1 \tag{39}$$

$$\pi_n = \frac{P_{t_9}}{P_{t_5}} = \exp\left(-\frac{s_9 - s_5}{R}\right) \tag{40}$$

The exit velocity can be obtained from the difference between the total and static enthalpies.

$$V_9 = \sqrt{2\left(h_{t9} - h_9\right)} \tag{41}$$

and for the fan exit nozzle we have:

$$\tau_{fn} = \frac{h_{t_{19}}}{h_{t_{13}}} = 1 \tag{42}$$

$$\pi_{fn} = \frac{P_{t_{19}}}{P_{t_{13}}} = \exp\left(-\frac{s_{19} - s_{13}}{R}\right) \tag{43}$$

The exit velocity can be obtained from the difference between the total and static enthalpies.

$$V_{19} = \sqrt{2\left(h_{t19} - h_{19}\right)} \tag{44}$$

The engine specific thrust can be obtained from adding the fan specific thrust to core engine specific thrust, we have:

$$\begin{aligned} \frac{F}{\overset{\circ}{m}_\circ} &= \frac{a_\circ}{(1+\alpha)}\left[(1+f)\frac{V_9}{a_\circ} - M_\circ + (1+f)\frac{R_t}{R_c}\frac{T_9/T_\circ}{V_9/a_\circ}\frac{1 - P_\circ/P_9}{\gamma_c}\right] \\ &+ \frac{\alpha\, a_\circ}{(1+\alpha)}\left[\frac{V_{19}}{a_\circ} - M_\circ + \frac{T_{19}/T_\circ}{V_{19}/a_\circ}\frac{1 - P_\circ/P_{19}}{\gamma_c}\right] \end{aligned} \tag{45}$$

and thrust specific fuel consumption

$$S = \frac{f}{(1+\alpha)F/\dot{m}_{\circ}} \tag{46}$$

Thermal efficiency is defined as

$$\eta_T = \frac{a_o^2\left[(1+f)(V_9/a_o)^2 + \alpha(V_{19}/a_o)^2 - (1+\alpha)M_o^2\right]}{2fh_{PR}} \tag{47}$$

The Propulsive efficiency is

$$\eta_P = \frac{2M_o\left[(1+f)(V_9/a_o) + \alpha(V_{19}/a_o) - (1+\alpha)M_o\right]}{\left[(1+f)(V_9/a_o)^2 + \alpha(V_{19}/a_o)^2 - (1+\alpha)M_o^2\right]} \tag{48}$$

The Overall efficiency is

$$\eta_o = \frac{TV_o}{\dot{Q}_{in}} = \eta_P\eta_T \tag{49}$$

Separate stream turbofan engines are generally used with subsonic aircraft and the pressure ratio across both primary and secondary nozzle is not very large. As a result, often-convergent only nozzles are utilized. In this case, if the nozzles are choked, we have:

$$\frac{P_{t19}}{P_{19}} = \left(\frac{\gamma_c+1}{2}\right)^{\gamma_c/(\gamma_c-1)} \text{ and } \frac{P_{t9}}{P_9} = \left(\frac{\gamma_t+1}{2}\right)^{\gamma_t/(\gamma_t-1)}$$

Thus

$$\frac{P_{\circ}}{P_{19}} = \frac{P_{t19}/P_{19}}{P_{19}/P_{\circ}} = \frac{\left[(\gamma_c+1)/2\right]^{\gamma_c/(\gamma_c-1)}}{\pi_r\pi_d\pi_F\pi_{Fn}} \tag{50}$$

and

$$\frac{P_{\circ}}{P_9} = \frac{P_{t9}/P_9}{P_9/P_{\circ}} = \frac{\left[(\gamma_t+1)/2\right]^{\gamma_t/(\gamma_t-1)}}{\pi_r\pi_d\pi_{cL}\pi_{cH}\pi_b\pi_{tH}\pi_{tL}\pi_n} \tag{51}$$

Table 3: Components Design Choice Parameters

Parameter	Selected value
Diffuser pressure ratio	0.98
Main burner pressure ratio	0.94
Fan exhaust nozzle pressure ratio	0.98
Core engine exhaust nozzle pressure ratio	0.98
Fan polytropic efficiency	0.89
Low-pressure compressor polytropic efficiency	0.9
High-pressure compressor polytropic efficiency	0.9
High-pressure turbine polytropic efficiency	0.9
Low-pressure turbine polytropic efficiency	0.9
Main burner combustion efficiency	0.98

If the nozzles are not choked we take $\mathbf{P_{19} = P_o}$ and / or $\mathbf{P_9 = P_o}$.

The performance data of the base line engine JT9D-7R turbofan engine at sea level static conditions as reported by the manufacture is given in [11-13]. The results of the design point calculations using aviation fuel are given in Table (**4**); it is show that there is a good correlation between the prediction engine performance parameters and the manufacture reported values. The predicted values of thrust and thrust specific fuel consumption are 236 kN, 9.93 g/ (N sec) respectively. The manufacture's thrust value at sea level static is 213-249 kN. It should be noticed that both the cold and hot nozzle streams are not choked.

Table 4: Engine and Engine Component Performance Parameters Using Aviation Fuel

Parameter	Predicted value
Specific thrust	312 N/kg
Thrust specific fuel consumption	9.93 g/(N.sec)
Air exit velocity from fan exhaust nozzle (V_{19})	302 m/sec
Combustion gases exit velocity (V_9)	357 m/sec
Fan isotropic efficiency	0.8805
Low-pressure compressor isotropic efficiency	0.8801
High-pressure compressor isotropic efficiency	0.8712
High-pressure turbine isotropic efficiency	0.9114
Low-pressure turbine isotropic efficiency	0.918
Engine thermal efficiency	36.21%

Table 5: Engine and engine component performance parameters using natural gas

Parameter	Predicted value
Specific thrust	321 N/kg
Thrust specific fuel consumption	8.55 g/(N.sec)
Air exit velocity from fan exhaust nozzle (V_{19})	302 m/sec
Combustion gases exit velocity (V_9)	405 m/sec
Fan isotropic efficiency	0.8805
Low-pressure compressor isotropic efficiency	0.8801
High-pressure compressor isotropic efficiency	0.8712
High-pressure turbine isotropic efficiency	0.91
Low-pressure turbine isotropic efficiency	0.9189
Engine thermal efficiency	38%

Engine performance parameters (specific thrust, thrust specific fuel consumption) are affected by the fuel lower calorific value. Since all calculations depend

on the fuel energy chart, slight increase on the specific thrust has been noticed 3% when using natural gas fuel.

This low increase of the specific thrust is due to engine design limits and components design choice parameters, since the engine already developed and components matched and design parameters optimized. Meanwhile the major effect on engine performance can be seen on the thrust specific fuel consumption. Since the thrust specific fuel consumption decreased when using natural gas by 14%. The decrease in the thrust specific fuel consumption is due to the fuel lower calorific value and engine design limits. Also the fuel to air ratio decreased by 11%, which means less pollutant effect.

3. PERFORMANCE ANALYSIS

The aircraft gas turbine engine is a very complex machine. The basic tools for modeling the engine performance are developed here based on work of Gordon Oates [13, 15]. All off-design calculations depend on satisfying essential conditions of compatibility of mass flow, work done and rotational speed between the various components. The variation of mass flow, pressure ratio and efficiency with rotational speed of the compressor and turbine is obtained from the compressor and turbine characteristics (maps). The following assumptions will be made in the turbofan performance analysis:

- The flow is choked at the high-pressure turbine entrance nozzle, low-pressure turbine entrance nozzle, the primary and bypass duct nozzles.
- The total pressure ratios of the main burner, primary exit nozzle, and bypass stream exit nozzle (π_b, π_n, π_{Fn}) do not change from their reference values.
- The component efficiencies (η_{cH}, η_{cL}, η_b, η_{tH}, η_{tL}, η_m) do not change from their reference values.
- Turbine cooling and leakage effects are neglected.
- No power is removed from the turbine to drive accessories.
- Gases will be assumed to be perfect both upstream and down stream of the main burner with average constant specific heats.
- Gases will be assumed to be perfect gases with the specific heat variable with the temperature through the main burner.

The dimensionless parameters useful in analyze complicated system analysis. The quantity of pressure and temperature are normally made dimensionless by dividing each by its receptive standard sea level static value. The dimensionless pressure is

$$\delta_i = \frac{P_{ti}}{P_{ref}} \tag{52}$$

$$\theta = \frac{T_{ti}}{T_{ref}} \tag{53}$$

$$m_{ci} = \frac{\overset{\circ}{m}_i \sqrt{\theta_i}}{\delta_i} \tag{54}$$

$$N_{ci} = \frac{N}{\sqrt{\theta_i}} \tag{55}$$

$$F_c = \frac{F}{\delta_o} \tag{56}$$

$$S_c = \frac{S}{\sqrt{\theta_o}} \tag{57}$$

The influence of the engine control system on compressor performance during change flight conditions and throttle setting can be understood from the following equations:

$$T_{to} = T_{ref}\frac{T_{to}}{T_{ref}} = T_{ref}\theta_o \tag{58}$$

$$\theta_o = \frac{T_o}{T_{ref}}\tau_r = \frac{T_o}{T_{ref}}\left(1 + \frac{\gamma - 1}{2} M_O^{\,2}\right) \tag{59}$$

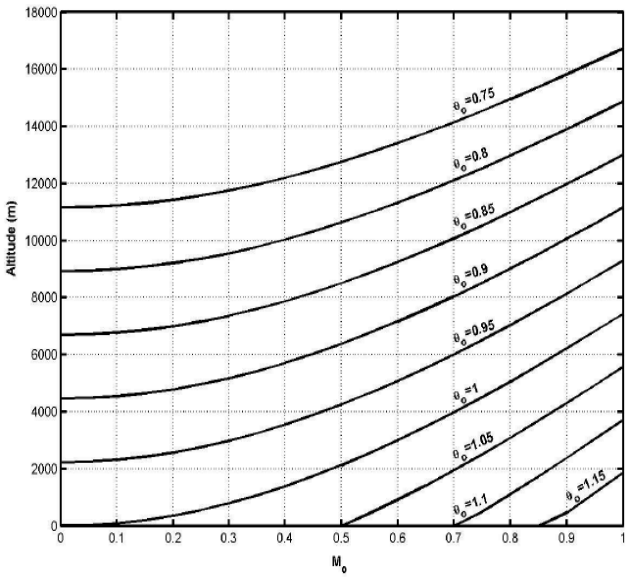

Figure 8: Temperature ratio versus Mach number and altitude.

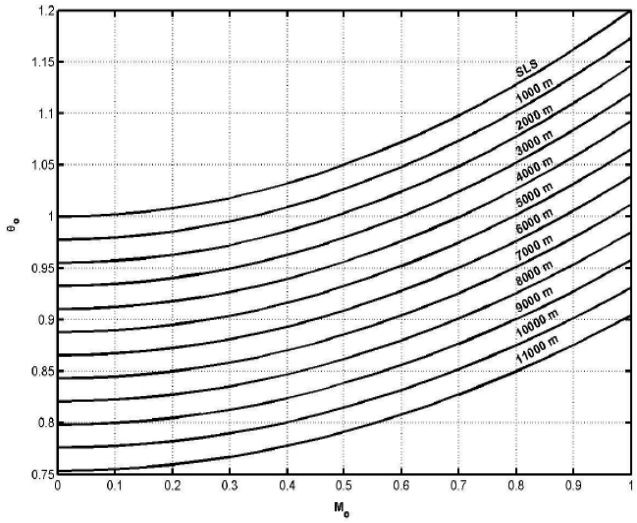

Figure 9: Temperature ratio versus Mach number at different altitude.

Equation (59) and Figures (**8**) and (**9**) show that θ_o include the influence of both the altitude (through the ambient temperature T_o) and the flight Mach number. The performance of a simple aero gas turbine depends on the operation of its gas generator. The corrected mass flow rate of the compressor is

$$\overset{\circ}{m}_{c2} = \left(\frac{T_{t2}}{T_{t4}}\right)^{1/2} \pi_c \pi_b \frac{P_{ref}}{\sqrt{T_{ref}}} \frac{A_4}{1+f} MFP(M_4) \tag{60}$$

Equation (60) is straight line on a compressor map for constant values of T_{t4}/T_{t2}, A_4, f and M_4. Lines of constant T_{t4}/T_{t2} are plotted on a typical compressor map in Figure (**10**) for constant A_4 and f. Station 4 chokes at pressure ratio of about 2 on Figure (**10**) where the lines are curved at low compressor pressure ratio from pressure ratio of 1 at corrected mass flow rate of 0. For the case when station 4 is choked

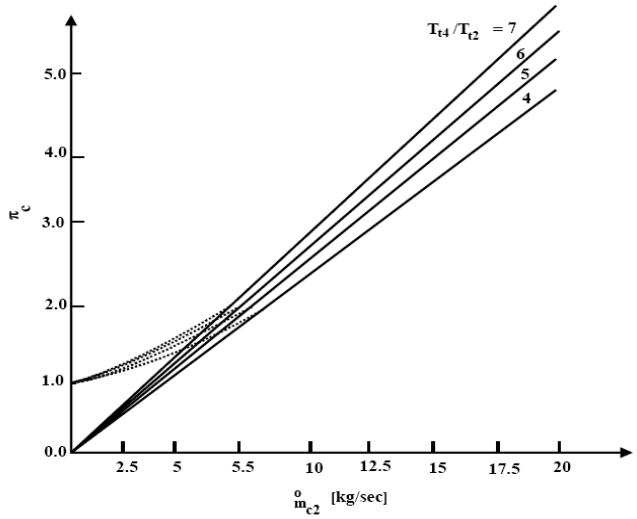

Figure 10: Compressor map with lines of constant T_{t4}/T_{t2}.

$$\overset{\circ}{m}_{c2} = C_1 \frac{\pi_c}{\sqrt{T_{t4}/T_{t2}}} \tag{61}$$

For a gas generator, the specific relationship between compressor pressure ratio and corrected mass flow rate is called the compressor operating line and depends on the characteristics of the turbine. From the work balance between the compressor and turbine, we get

$$\pi_c = \left\{1 + \frac{T_{t4}}{T_{t2}}\left[\frac{Cp_t}{Cp_c}\eta_c\eta_m(1+f)(1-\tau_t)\right]\right\}^{\gamma_c/(\gamma_c-1)} \tag{62}$$

The term in the square bracket can be considered constant when τ_t is constant. The equation for compressor operating line is

$$\overset{\circ}{m}_{c2} = \frac{\pi_c}{\sqrt{(\pi_c^{((\gamma_c-1)/\gamma_c)}-1)}} \frac{C_1}{\sqrt{C_2}} \text{ for constant } \tau_t \tag{63}$$

From the fact that $T_{t2} = T_{to}$, we can write equation (62) as

$$\pi_c = \left(1 + \frac{T_{t4}}{\theta_o} k_1\right)^{\gamma_c/(\gamma_c-1)} \tag{64}$$

Where k_1 is a constant can be found from substituting in equation (64) with reference conditions (design point), and equation (64) can be plotted as shown in Figure (**11**).

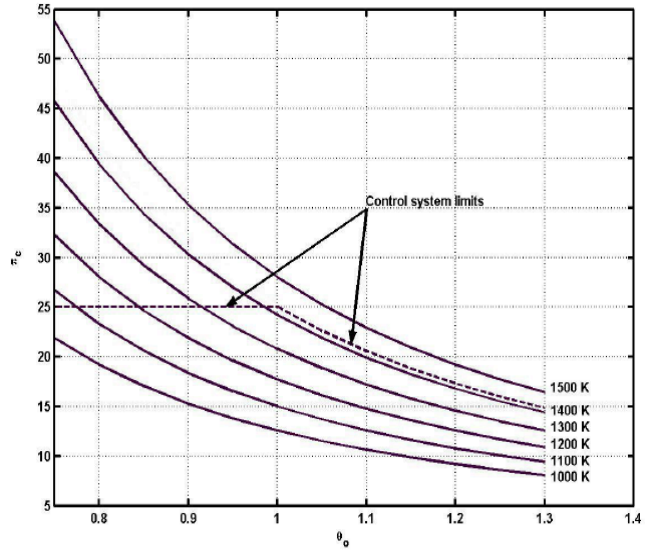

Figure 11: Compressor pressure ratio versus temperature ratio.

Figures (**8, 9, 11**) and (**12**) represent the influence of engine control system on the gas generator. For

example at the reference point (design point) for $\mathbf{M_o}$ = 0 at sea level using Figure (**8**) or Figure (**9**) the value of $\boldsymbol{\theta_o}$ can be obtained, $\boldsymbol{\theta_o}$ = 1. Figure (**11**) shows the engine control limits. Maximum compressor pressure ratio $\boldsymbol{\pi_c}$ =25, and maximum inlet temperature to the turbine $\mathbf{T_{t4}}$ = 1422K. Figure (**12**) shows the engine corrected mass flow rate and maximum inlet turbine temperature 1422K. Using the value of the determined $\boldsymbol{\theta_o}$ indicates, which limit would be used to control the engine performance either the maximum compressor pressure ratio or maximum inlet temperature to the turbine.

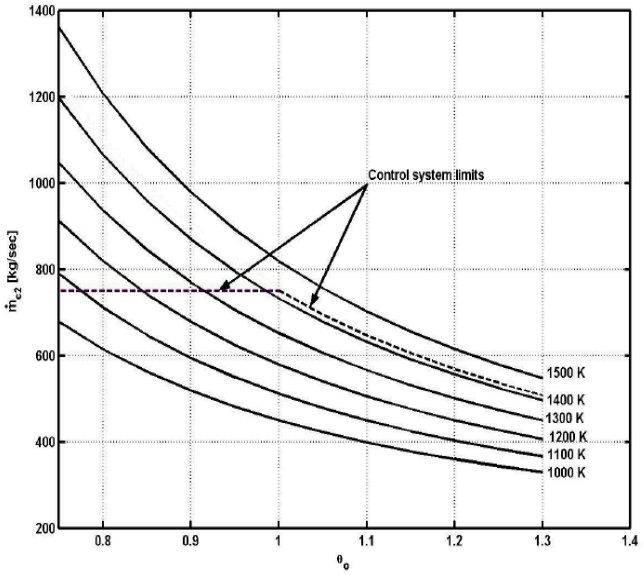

Figure 12: Corrected mass flow rate versus temperature ratio.

The maximum compressor pressure ratio controls the engine performance when $\boldsymbol{\theta_o} \leq 1$, and gives the corresponding line of maximum inlet temperature to turbine $\mathbf{T_{t4}}$. The maximum inlet temperature to the turbine controls engine performance when $\boldsymbol{\theta_o} \geq 1$, and gives the corresponding compressor pressure ratio. For the case of $\boldsymbol{\theta_o}$ =1 that means either control limit can be used. When the engine flight condition changed, for example to $\mathbf{M_o}$ = 0.8 and altitude of 10000m. Then from Figure (**8**) or Figure (**9**) we get $\boldsymbol{\theta_o}$ = 0.86, and from Figure (**11**) we know that the engine controlled by the maximum engine compressor pressure ratio, and the maximum inlet temperature to the turbine is 1220K. Which is convenient because, this altitude is nearly the cruise altitude that the engine thrust specific fuel consumption is minimum and engine thrust also reduced, and to achieve that T_{t4} must be reduced. Due to the assumptions made, the choked flow at station 4 and 4.5 of high-pressure spool during engine operation requires:

Constant value of π_{tH}, τ_{tH}, $\dot{m}_{c}4$, $\dot{m}_{c}4.5$

The performance relationship for engine components developed as follow:

For the High-pressure turbine:

$$\dot{m}4 = \frac{P_{t4}}{\sqrt{T_{t4}}} A_4 MFP(M_4) = \dot{m}4.5 = \frac{P_{t4.5}}{\sqrt{T_{t4.5}}} A_{4.5} MFP(M_{4.5}) \quad (65)$$

Using the assumptions made:

$$\frac{P_{t4.5}/P_{t4}}{\sqrt{T_{t4.5}/T_{t4}}} = \frac{\pi_{tH}}{\sqrt{\tau_{tH}}} = \textbf{Constant}. \quad (66)$$

Thus for constant $\boldsymbol{\eta_{tH}}$, we have Constant value of $\boldsymbol{\pi_{tH}}$, $\boldsymbol{\tau_{tH}}$, $\dot{m}_{c}4$, $\dot{m}_{c}4.5$

for Low-pressure turbine:

$$\pi_{tL} = \pi_{tLR} \sqrt{\frac{\tau_{tL}}{\tau_{tLR}}} \frac{MFP(M_{9R})}{MFP(M_9)} , \boldsymbol{f(\tau_{tL}, M_9)} \quad (67)$$

Where

$$\tau_{tL} = 1 - \eta_{tL}\left(1 - \pi_{tL}^{\left((\gamma_t - 1)/\gamma_t\right)}\right) , \boldsymbol{f(\pi_{tL})} \quad (68)$$

For The low-pressure spool: we can write:

$$\tau_{cL} = 1 + (\tau_F - 1)\frac{\tau_{cLR} - 1}{\tau_{FR} - 1} , \boldsymbol{f(\tau_{fL})} \quad (69)$$

The pressure ratio for the low-pressure compressor is given by:

$$\pi_{cL} = \left[1 + \eta_{cL}(\tau_{cL} - 1)\right]^{\gamma_c/(\gamma_c - 1)} , \boldsymbol{f(\tau_{cL})} \quad (70)$$

An expression for the engine bypass ratio at any operating conditions is obtained by relating the mass flow rates of the core engine and fan stream to their reference values.

$$\alpha = \alpha_R \frac{\pi_{cLR}\pi_{cHR}/\pi_{FR}}{\pi_{cL}\pi_{cH}/\pi_F} \sqrt{\frac{\tau_\lambda/(\tau_r\tau_F)}{\left[\tau_\lambda/(\tau_r\tau_F)\right]_R}} \frac{MFP(M_{19})}{MFP(M_{19R})} , \boldsymbol{f(\tau_f, \pi_{cH}, M19)} \quad (71)$$

Engine mass flow rate $\dot{m}_o$: the engine mass flow rate can be written as:

$$\dot{m}_O = \dot{m}_{OR} \frac{1+\alpha}{1+\alpha_R} \frac{P_o \pi_r \pi_d \pi_{cLr} \pi_{cH}}{(P_o \pi_r \pi_d \pi_{cLr} \pi_{cH})_R} \sqrt{\frac{T_{t4R}}{T_{t4}}} \quad (72)$$

From the power balance of high-pressure spool

$$\tau_{cH} = 1 + \frac{T_{t4}/T_o}{\left(T_{t4}/T_o\right)_R} \frac{\left(\tau_r \tau_{cL}\right)_R}{\tau_r \tau_{cL}} \left(\tau_{cH} - 1\right)_R \text{, } f(\tau_{cL}) \tag{73}$$

The pressure ratio of the high-pressure compressor is given by:

$$\pi_{cH} = \left[1 + \eta_{cH}\left(\tau_{cH} - 1\right)\right]^{\gamma_c/\left(\gamma_c - 1\right)} \text{, } \boldsymbol{f(\tau_{cH})} \tag{74}$$

$$\tau_F = 1 + \left(\tau_{FR} - 1\right)\left[\frac{1 - \tau_{tL}}{\left(1 - \tau_{tL}\right)_R} \frac{\tau_\lambda/\tau_r}{\left(\tau_\lambda/\tau_r\right)_R} \frac{\tau_{cLR} - 1 + \alpha_R\left(\tau_{FR} - 1\right)}{\tau_{cLR} - 1 + \alpha\ \left(\tau_{FR} - 1\right)}\right]$$
$$\text{, } \boldsymbol{f(\tau_{tL}, \alpha)} \tag{75}$$

The cold nozzle exit Mach number is given by

$$M_{19} = \sqrt{\frac{2}{\gamma_c - 1}\left[\left(\frac{P_{t19}}{P_{19}}\right)^{\left(\gamma_c - 1\right)/\gamma_c} - 1\right]} \text{, } \boldsymbol{f(\pi_f)} \tag{76}$$

The core engine nozzle Mach number is given by

$$M_9 = \sqrt{\frac{2}{\gamma_t - 1}\left[\left(\frac{P_{t9}}{P_9}\right)^{\left(\gamma_t - 1\right)/\gamma_t} - 1\right]} \text{, } \boldsymbol{f(\pi_f,\ \pi_{cH},\ \pi_{tL})} \tag{77}$$

The Mass Flow Parameter for a calorically perfect gas is given by

$$MFP(M) = \frac{\overset{\circ}{m}\sqrt{T_t}}{P_t A} = \frac{M\sqrt{\gamma/R}}{\left\{1 + \left[\left(\gamma - 1\right)/2\right]M^2\right\}^{(\gamma+1)/[2(\gamma-1)]}} \tag{78}$$

The specific thrust of the JT9D-7R turbofan engine is given by

$$\frac{F}{\overset{\circ}{m}_o} = \frac{a_o}{1+\alpha}\left[\left(1+f\right)\frac{V_9}{a_o} - M_o + \left(1+f\right)\frac{R_t}{R_c}\frac{T_9/T_o}{V_9/a_o}\frac{1 - P_o/P_9}{\gamma_c}\right]$$
$$+ \frac{a_o \alpha}{1+\alpha}\left[\frac{V_{19}}{a_o} - M_o + \frac{T_{19}/T_o}{V_{19}/a_o}\frac{1 - P_o/P_{19}}{\gamma_c}\right] \tag{79}$$

and the thrust specific fuel consumption is given by

$$S = \frac{f}{\left(1+\alpha\right)\left(F/\overset{\circ}{m}_o\right)} \tag{80}$$

$$T_{t3} = T_o\ \tau_r\ \tau_{cL}\ \tau_{cH} \tag{81}$$

From the fuel temperature – entropy chart at excess air factor $\boldsymbol{\lambda = \infty}$, the value of the $\mathbf{h_{t3}}$ can be predicted. Also from the engine, control system the maximum inlet temperature to turbine $\mathbf{T_{t4}}$ determined, and from the interpolation between the excess air factor and enthalpies, the value of the $\mathbf{h_{t4}}$ can be predicted.

The value of fuel to air ratio can be predicted as follows

$$f = \frac{h_{t4} - h_{t3}}{\eta_b h_{PR} - h_{t4}} \tag{82}$$

The variation in engine mechanical speed can be predicted from Euler pump equation for calorically perfect gas.

$$\left(\frac{N}{N_R}\right)_{Fan} = \sqrt{\frac{T_o \tau_r\left(\pi_f^{\left(\gamma_c - 1\right)/\gamma_c} - 1\right)}{\left[T_o \tau_r\left(\pi_f^{\left(\gamma_c - 1\right)/\gamma_c} - 1\right)\right]_R}} \tag{83}$$

For high-pressure spool

$$\left(\frac{N}{N_R}\right)_{HPspool} = \sqrt{\frac{T_o \tau_{cL}\left(\pi_{cH}^{\left(\gamma_c - 1\right)/\gamma_c} - 1\right)}{\left[T_o \tau_{cL}\left(\pi_{cH}^{\left(\gamma_c - 1\right)/\gamma_c} - 1\right)\right]_R}} \tag{84}$$

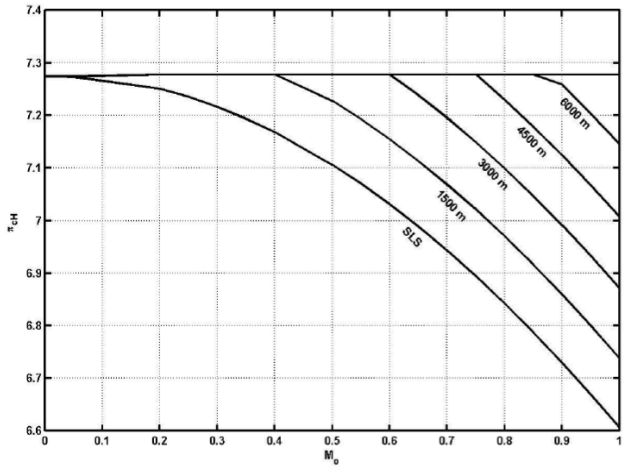

Figure 13: High-pressure compressor pressure ratio of JT9D-7R turbofan engine at maximum thrust using aviation fuel.

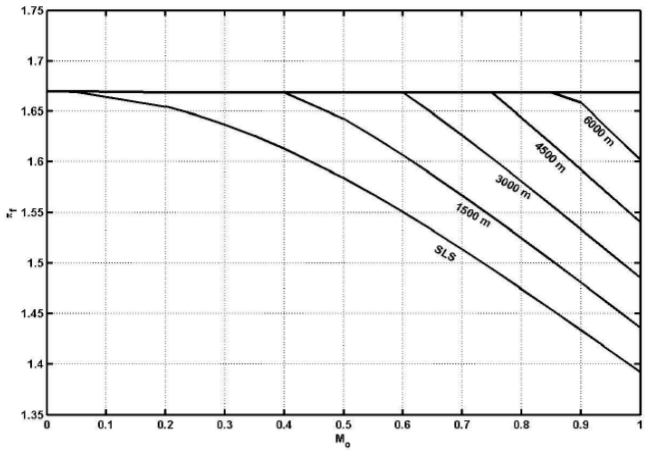

Figure 14: Fan pressure ratio of JT9D-7R turbofan engine at maximum thrust using aviation fuel.

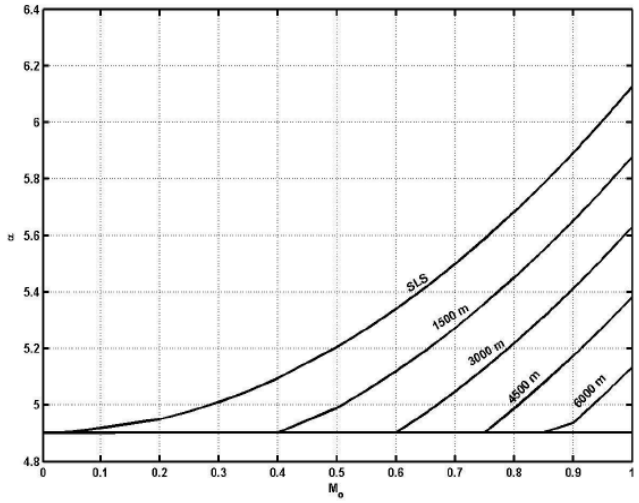

Figure 15: Bypass ratio of JT9D-7R turbofan engine at maximum thrust using aviation fuel.

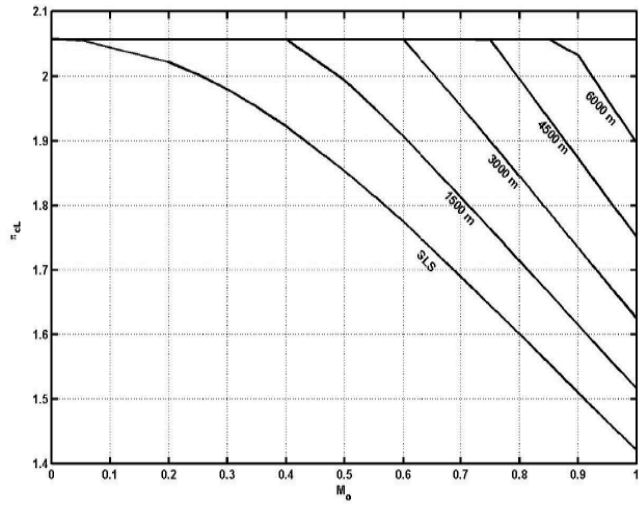

Figure 16: Low-pressure compressor -pressure ratio of JT9D-7R turbofan engine at maximum thrust using aviation fuel.

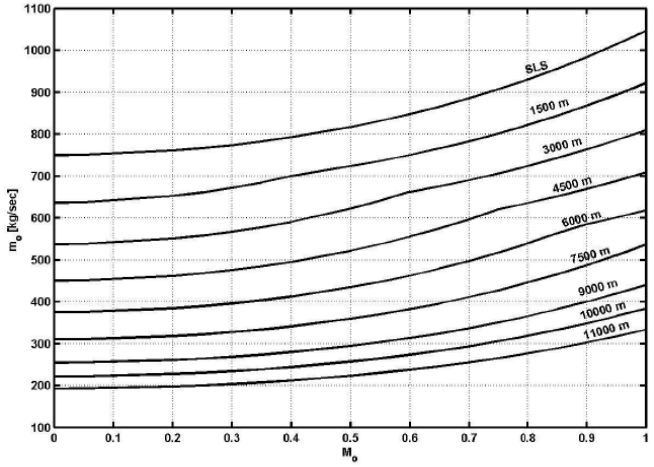

Figure 17: Engine inlet mass flow rate of JT9D-7R turbofan engine at maximum thrust using aviation fuel.

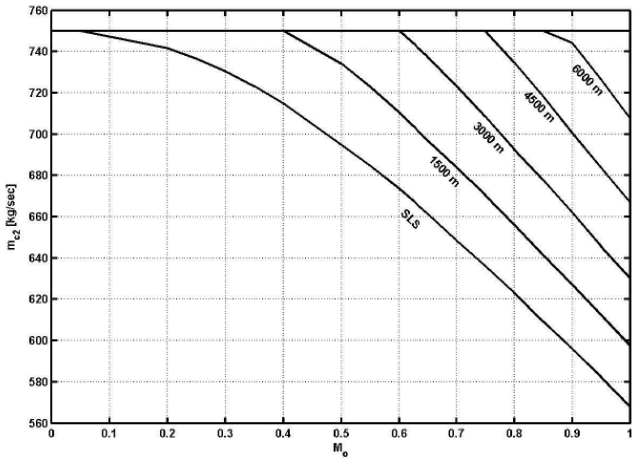

Figure 18: Engine inlet corrected mass flow rate of JT9D-7R turbofan engine at maximum thrust using aviation fuel.

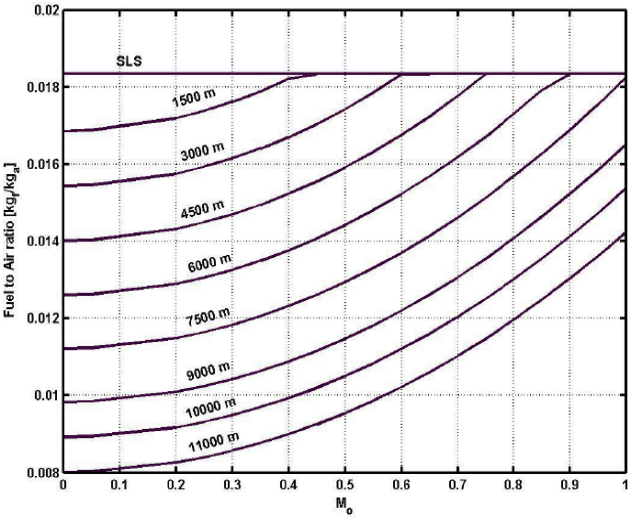

Figure 19: Fuel to Air ratio of JT9D-7R turbofan engine using aviation fuel.

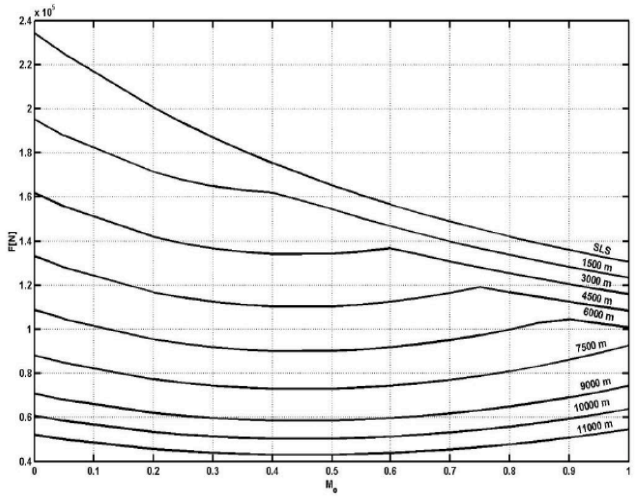

Figure 20: Maximum thrust of JT9D-7R turbofan engine using aviation fuel.

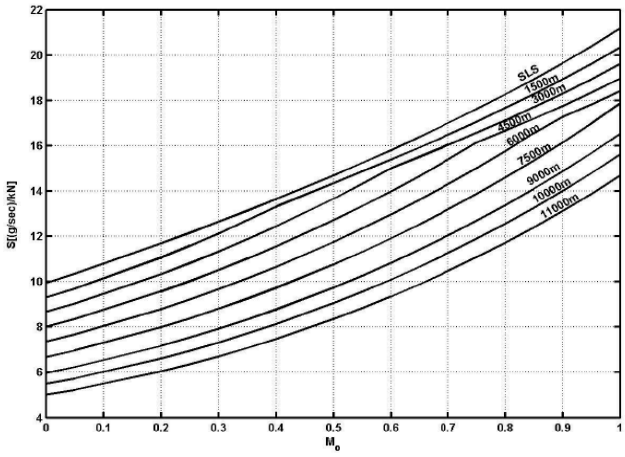

Figure 21: Thrust specific fuel consumption of JT9D-7R turbofan engine at maximum thrust using aviation fuel.

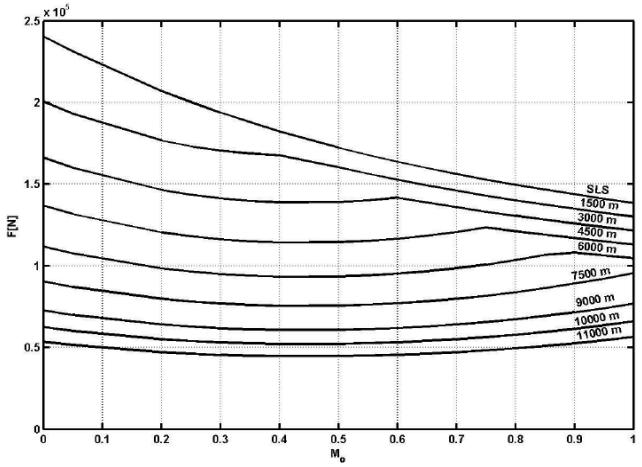

Figure 24: Maximum thrust of JT9D-7R turbofan engine using natural gas fuel.

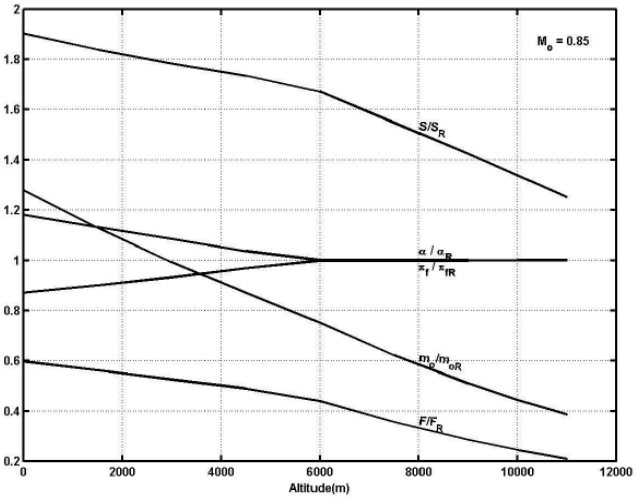

Figure 22: Effect of altitude on JT9D-7R turbofan engine at maximum thrust using aviation fuel.

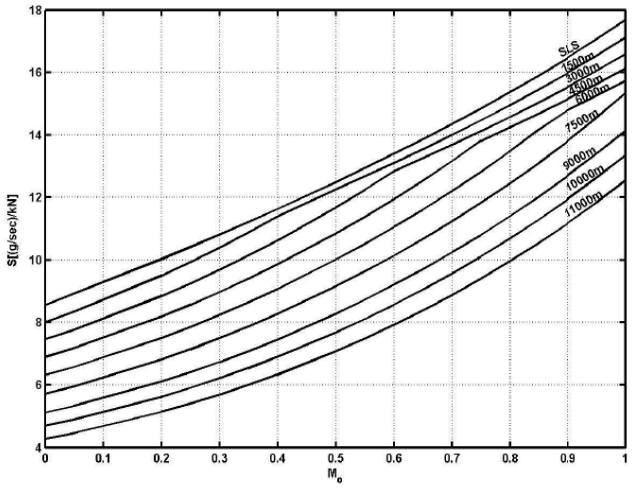

Figure 25: Thrust specific fuel consumption of JT9D-7R turbofan engine at maximum thrust using natural gas fuel.

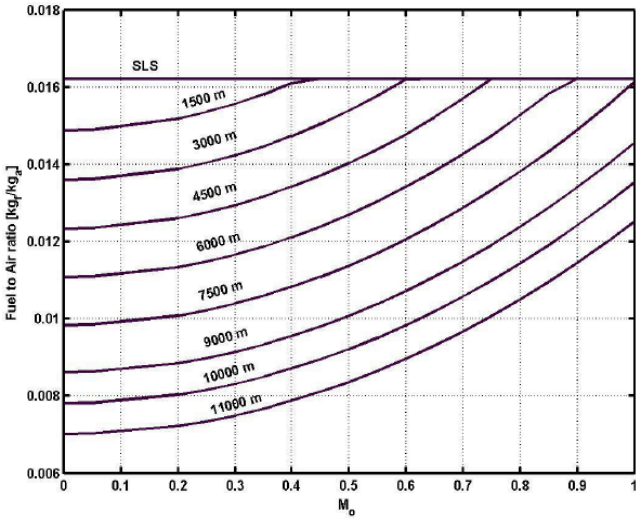

Figure 23: Fuel to Air ratio of JT9D-7R turbofan engine using natural gas fuel.

The high-pressure compressor pressure ratio of Figure (**13**) has the same trend with Mach number and altitude as the fan pressure ratio of Figure (**14**), the low-pressure compressor pressure ratio of Figure (**16**) and the corrected engine mass flow rate of Figure (**18**). The corrected mass flow rate, the low-pressure compressor pressure ratio and the high-pressure compressor pressure ratio reach their maximum values when the bypass stream is choked. Figure (**15**) shows that the engine bypass ratio at maximum thrust has a constant minimum value of about 4.9 when the bypass stream is choked. The fuel to air ratio and high-pressure spool mechanical speed has the same trend with Mach number and altitude. Figure (**19**) shows that the fuel air ratio reaches its maximum value when the bypass ratio reaches its minimum value of about 4.9 when the bypass stream is choked. The effect of altitude on engine performance at maximum thrust at

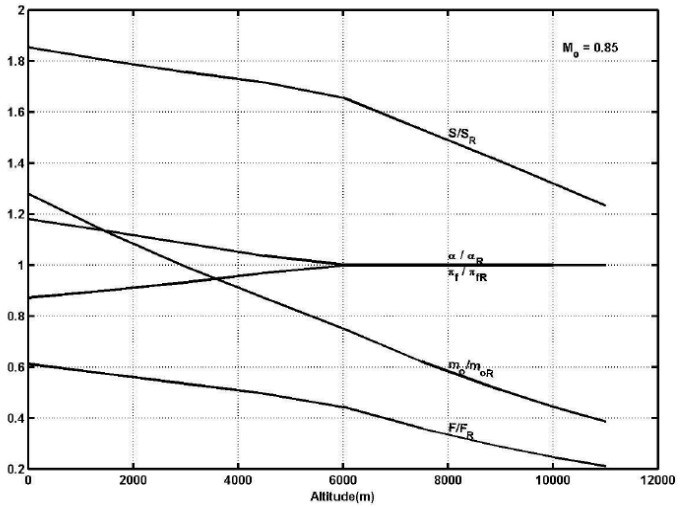

Figure 26: Effect of altitude on JT9D-7R turbofan engine at maximum thrust using natural gas fuel.

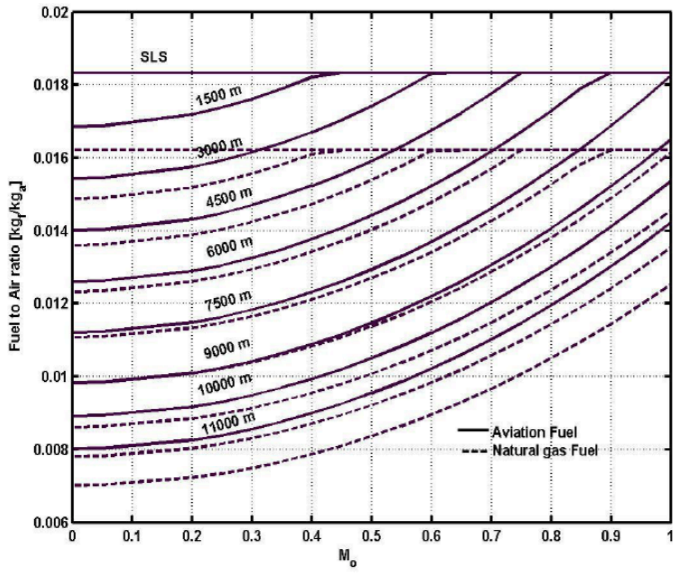

Figure 27: Fuel to Air ratio of JT9D-7R turbofan engine using aviation and natural gas fuels.

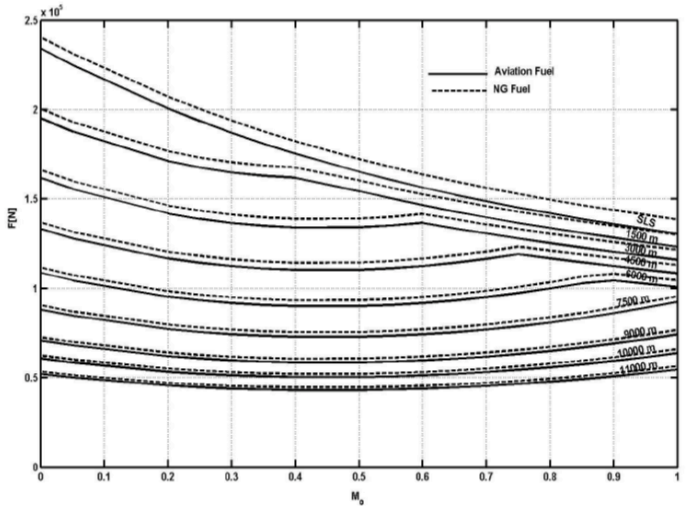

Figure 28: Maximum thrust of JT9D-7R turbofan engine using aviation and natural gas fuels.

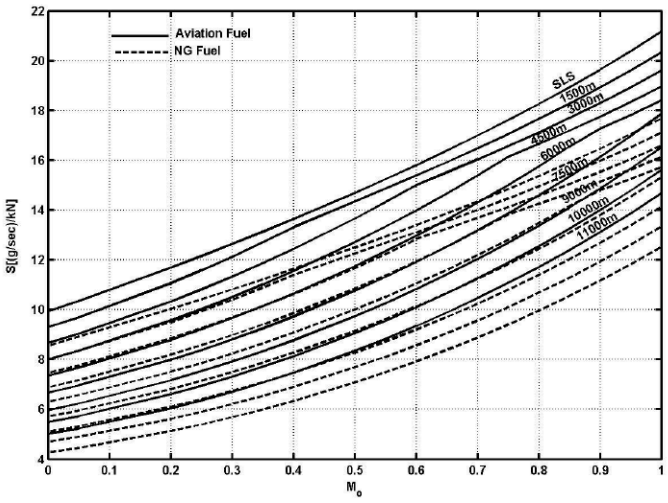

Figure 29: Thrust specific fuel consumption of JT9D-7R turbofan engine using aviation and natural gas fuels.

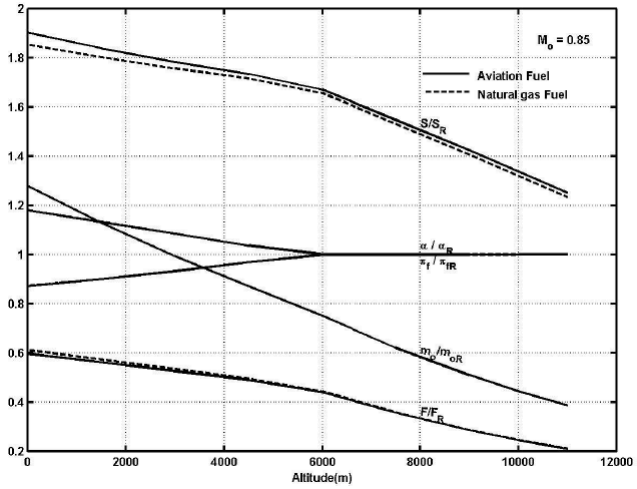

Figure 30: Effect of altitude on JT9D-7R turbofan engine at maximum thrust using aviation and natural gas fuels.

0.85 Mach number is shown in Figure (**22**). The decrease in engine thrust, fuel consumption, and air mass flow rate with altitude are shown in Figure (**22**). The variations of high-pressure compressor pressure ratio, fan pressure ratio, bypass ratio, low-pressure compressor pressure ratio, engine mass flow rate, engine corrected mass flow rate, fan mechanical speed and high-pressure spool mechanical speed with Mach number and altitude, respectively when using natural gas fuel have same trend of performance curves as in aviation fuel. Choking value also the same as aviation fuel. Figure (**23**) shows that the fuel to air ratio using natural gas fuel is lower than aviation fuel to air ratio but has same trend. The maximum thrust and thrust specific fuel consumption performance curves Figure (**24**) and (**25**) have the same trend as for aviation fuel. The thrust slightly increased by 3% and the thrust specific fuel consumption decreased by 14% at sea level static conditions. At cruise conditions the maximum thrust increased by 3.5% and the thrust specific fuel consumption by 15%. Also the effect of altitude on engine performance at maximum thrust at 0.85 Mach number is shown in Figure (**26**). The decrease in engine thrust, fuel consumption, and air mass flow rate with altitude are shown in Figure (**26**). Figure (**27**) through (30) summarize the above discussion. In Figure (**27**) the lines of fuel to air ratio when using natural gas has been add to fuel to air ratio when using aviation fuel. In Figure (**28**) the lines of specific thrust when using natural gas add to the lines of specific thrust when using conventional aviation fuel. In Figure (**29**) the lines of thrust specific fuel consumption when using natural gas add to the lines of thrust specific fuel consumption when using conventional aviation. These Figures show the major effect of fuel type on engine performance parameters.

Also in Figure (**30**), the lines represent the effect of altitude on the engine performance parameters when using natural gas fuel has been added to the lines of altitude effect when using conventional aviation fuel. Figure (**30**) shows also that the major effect of using natural gas fuel was in the thrust specific fuel consumption.

CONCLUSIONS

A computerized prediction of the design point calculations based on sea level static conditions of the base line engine JTT9D-7R double spool turbofan engine is carried out. The calculations are based on computerized temperature-entropy charts per mole combustion gases. The computer program is designed with sufficient generality to include excess air factor variations and temperature variations. The computer run results are compared with the manufacture reported data. The computer program was used also to predict the design point calculations using natural gas fuel. The results show that the specific thrust increased by 3% and the thrust specific fuel consumption decreased by 14%, also the fuel to air ratio decreased by 11%.

A computerized performance prediction of base line engine JT9D-7R turbofan engine is carried out at different altitude and Mach number using aviation fuel and natural gas fuel respectively. The calculations are carried out assuming perfect gases up stream and down stream of main burner. The variations of temperature and excess air factor are taken into account through the main burner. The results show that the thrust increased by 3% and the thrust specific fuel consumption decreased by 14% at sea level static conditions, and the thrust increased by 3.5% and the thrust specific fuel consumption decreased by 15% at cruise conditions.

NOMENCLATURE

Symbol	Unit	Description
A	m^2	Cross-section area
a	m/sec	Sound speed, fuel carbon content
b		Fuel hydrogen content
Cp	kJ/kmol K	Specific heat at constant pressure
Cv	kJ/kmol K	Specific heat at constant volume
e		Polytropic efficiency
EXP		Exponential
F	N	Uninstalled thrust, thrust
f	kg_f/kg_a	Fuel/air ratio
h	kJ/kmol	Specific enthalpy
K		Constant
LCV	kJ/kg_f	Fuel lower calorific value
LNG		Liquid natural gas
$\overset{\circ}{m}$	kg/sec	Mass flow rate
M	kg/kmol,-	Molecular weight, Mach number
M_f	$kmol_{cg}/kg_f$	Number of moles of combustion gases per kg fuel
MFP		Mass flow parameter
n	mole	Number of moles of any species
N	rpm	Engine revolution
P	Pa	Pressure
R	kJ/kmol K,	Universal gas constant=8.314, radius
S	g/N sec	Specific thrust fuel consumption
s	kJ/kmol K	Specific entropy
T	K,N	Temperature, aircraft thrust
t	sec, m	Time, thickness
TSFC	mg/N sec	aircraft thrust specific fuel consumption
u	kJ/kmol	Specific internal energy
V	m^2, m/sec	Volume, velocity
$\overset{\circ}{W}$	kJ/sec	Power
W	N	Weight

Greek letter

Symbol	Unit	Description
Σ		Sum
α	-, rad	Bypass ratio, Angle of attack
γ		Ratio of specific heats
δ		Dimensionless pressure
η		Efficiency
θ		Dimensionless temperature
λ		Excess air factor

π		Pressure ratio
ρ	kg/m^3	Density
τ		Enthalpy ratio, temperature ratio
τ_λ		Enthalpy ratio or temperature ratio at burner exit
χ		Mole Fraction of species

Subscript

Symbol	**Description**
1,2,3,…	State points
b	Burner
c	Compressor, corrected
cH	High-pressure compressor
cL	Low-pressure compressor
d	Diffuser
f	Fuel, fan
fn	Fan nozzle
m	Mechanical
max	Maximum
min	Minimum
n	Nozzle
o	Initial, Stagnation
p	Constant pressure
r	Ram
ref	Reference Conditions
SLS	Sea level static
t	Total
tH	High-pressure turbine
tL	Low-pressure turbine
v	Constant volume
HPspool	High-pressure spool

REFERENCES

[1] Penner JE, Lister DH, Griggs DJ, Dokken DJ, McFarland M. Aviation and the global atmosphere. Intergovernmental Panel on Climate Change special report (IPCC). IBSN: 92-169; 1999.

[2] Abdelfattah AII, Abdelfattah H. The future role of natural gas in the Arab world. Faculty of Engineering Press, Alexandria, 1996.

[3] Kinoshita Y, Kitajima J, Shiraha M, Tatara A. Combustion study on methane-fuel Laboratory Scaled Ram Combustor, ASME PAPER 92-GT-413, 1992.

[4] Ivliev AV, Knysh IA, Lukachev VP. The effect of the structural features of a combustion chamber on the emission of toxic compounds. Aviatsionnaia Tekhnika Volume: 20, 1977.

[5] Khristich VA, Liubchik GN, Didenko VI, Shevchenko AM, Ilchenko VA. Energy characteristics of the combustion chambers of an aircraft engine when operating on natural gas. Energetika 1984; 72-77.

[6] Tumanovskii AG, Kovalev VN, Skuridin VG, Mingaleev FM. Testing the annular combustion chamber of the NK-8 aircraft engine using natural gas. Teploenergetika 1976.

[7] Lukachev SV, Rozno VG. Release of benz (a)pyrene with the exhaust gases of gas turbine engines burning natural gas. Aviatsionnaia Tekhnika 1991; 1(19): 98-100.

[8] Brewe GD. Hydrogen aircraft technology. CRC Press, Boca Raton page 3 1991.

[9] Kutakhov VP, Reznikov ME. To the problem of cryogenic aviation-aerospace engineering. Airforce Technical University 1999.

[10] Thomas CE, *et al*. Societal Impacts of fuel options for fuel cell vehicles. SAE: 982496 1998.

[11] The aircraft gas turbine and its operation, PWA, OI 200, East Hartford CT 1974.

[12] Jackson P. Jane's all Worlds aircraft 1960-1969. Jane's information group limited, sentinel house. UK. ISBN 0710618611 1970.

[13] Mattingly JD. Elements of gas turbine propulsion. McGraw Hill Inc. NY ISBN: 1996; 0-07-114521-4.

[14] Ferguson CR. Internal combustion engines. Applied theromsciences. John Wiley & Sons. New York, Chichester, Britsbane, Singapore 1978.

[15] Oates GO. Aerothermodynamics of gas turbine and rocket propulsion. Revised and enlarged version. AIAA education series. AIAA. WA 1988.

Received on 15-11-2014 Accepted on 25-11-2014 Published on 23-01-2015

DOI: http://dx.doi.org/10.15377/2409-9848.2014.01.02.1